TUDelft

Delft University of Technology

Jet noise prediction

Validation and physical insight

Van Der Velden, Wouter C.P.; Casalino, Damiano; Gopalakrishnan, Pradeep; Jammalamadaka, Avinash; Li, Yanbing; Zhang, Raoyang; Chen, Hudong

Important note
To cite this publication, please use the final published version (if applicable).
Please check the document version above.

Jet Noise Prediction: Validation and Physical Insight

W.C.P. van der Velden[*]

Exa GmbH, 4 Curiestraße, 70563, Stuttgart, Germany

D. Casalino[†]

Delft University of Technology, 1 Kluyverweg, 2629, Delft, The Netherlands

P. Gopalakrishnan[‡] A. Jammalamadaka[§] Y. Li[¶] R. Zhang[||] H. Chen[**]

Exa Corporation, 55 Network Drive, 01803, Burlington, Massachusetts

A hybrid Lattice-Boltzmann Model (LBM) Very Large Eddy Simulation (VLES) solver for high-speed non-isothermal subsonic flows is used to simulate the unsteady jet flow exhausting from a single axi-symmetric nozzle, as well as the associated noise spectra and directivity. The jet exit Mach number and temperature ratio are set according to the various setpoints from the NASA SMC000 experimental campaign. Both isothermal and heated core flows are considered. The far-field noise is computed through a Ffowcs-Williams and Hawkings (FW-H) analogy applied to a fluid surface encompassing the jet plume. Both time- and frequency-domain formulations are used, the latter in combination with an azimuthal Fourier transform of the linear source terms to analyze the contribution of the different azimuthal components. A resolution study is carried out for both aerodynamic and acoustic results. The near- and far-field results confirm that the underlying flow features and noise mechanisms are fully represented by the numerical solution. A physical analysis of the source mechanisms for a heated core case is performed through a wavelet decomposition applied to the turbulent flow to separate the coherent flow motion, usually attributed to the hydrodynamic fluctuations, and the chaotic perturbations, which have a more dominant acoustic character. The two separated contributions extracted from the flow on the FW-H surface are used to compute the corresponding far-field acoustic contributions. Interestingly, noise is practically generated only by the coherent flow motion. Finally, the frequency-domain FW-H formulation is used to analyze the different azimuthal flow perturbation modes. Strong convection effect along the various modes are found.

I.   Introduction

Recent turbofan design trends are expected to reduce the relative contribution of the jet to the overall aircraft noise of conventional under-wing civil aircraft configurations. In order to take advantage of the airframe noise shielding effects, future low-noise/low-boom supersonic commercial aircraft designs are oriented towards top-mounted engines.[1] Both for under-wing and top-mounted engine configurations, the interaction between the jet and parts of the airframe can have a crucial effect on the far-field noise levels. Indeed, for a conventional aircraft in high-lift conditions, the jet-flap interaction can produce a non-negligible contribution,[2] despite what usually assumed in preliminary design phases. For top-mounted engine aircraft, the fan noise radiated from the engine intake and exhaust can be reflected upward by the airframe, however the aft-body jet sources undergo a significantly lower shielding. For these reasons and others related to the

---

[*]Senior Aerospace Application Engineer, `wouter@exa.com`, AIAA member
[†]Professor, Aeroacoustics & Aerodynamics, Wind Energy, AIAA member
[‡]Senior Consulting Engineer
[§]Senior Validation Engineer
[¶]Senior Consulting Engineer
[||]Managing Director
[**]CSO

American Institute of Aeronautics and Astronautics

need of reducing the environmental cost of air transportation, jet noise will remain a relevant problem for the aircraft industry and the aeroacoustic community.

Predicting jet surface interaction is a challenging problem for current Computational Fluid Dynamics (CFD) technology, mostly due to the challenge of using high-order methods in the presence of complex geometries, while keeping the computational costs within reasonable limits. A variety of accurate Large Eddy Simulations (LES) of isolated jets have been reported in the literature,[3] and the geometrical complexity is limited to including the nozzle duct in the simulation.[4] More recently, hybrid Reynolds Averaged Navier-Stokes (RANS) LES models have been successfully used to simulate round jets[5] using a high-order structured mesh solver. The same technology, in combination with an overset structured multi-block technique has been used to simulate the turbulent-resolved flow field of a full annulus fan-stage system.[6] This constitutes an important achievement towards the capability of simulating full engine installation noise for complex geometries, with adequate accuracy. However, the computational time is still an issue for most CFD solvers based on the solution of flow governing equations using Partial Differential Equation (PDE) discretization techniques. A computationally more efficient alternative to classical PDE-based methods is constituted by the Lattice-Boltzmann Method (LBM). More specifically, Exa's LBM-VLES solver PowerFLOW has been successfully used in the past in the field of aircraft aeroacoustics at both component[7–9] and full aircraft level.[10,11] As a matter of fact, the same fan broadband noise prediction study carried out by Shur *et al*[6] was previously carried out by Casalino *et al*[9,12] who reported one order of magnitude faster computations for a similar accuracy level.

Very recently, some modifications of the physical kernel of PowerFLOW have been introduced with the goal, among others, of improving the robustness of the solver in the presence of heated unsteady flows and abrupt changes of the mesh resolution in regions of high flow non-uniformity. This is a situation that is typically encountered in aircraft-installed engine simulations. There is therefore the need to perform and report a fundamental validation of the new version of the solver for jet noise simulations. Measurements carried out by NASA with the SMC000 nozzle have been selected as a reference[13,14] for the validation purposes of the present work. Different cold and heated exhaust flow conditions are aerodynamically analyzed. In addition, the acoustic far-field is computed using both time- and frequency-domain integral formulations of the Ffowcs-Williams and Hawkings equation[15] applied to a permeable fluid surface encompassing the plume. A resolution study is carried out for both aerodynamic and acoustic results.

Performing a CFD validation study without any new physical insight is a missed opportunity. Therefore, the second and more original contribution of this work consists in analyzing some fundamental features of sound generation mechanisms in jets. Two techniques are served to this goal. A frequency-domain FW-H formulation is used[16] with the intent of investigating the radiation properties of the different time-azimuthal Fourier components and their relative contribution to the overall noise. Secondly, a wavelet-based decomposition techniques[17] is employed to separate the coherent part of the flow motion, which is usually attributed to the hydrodynamic instability waves, from the chaotic part, which has a more acoustic character. Interesting observations are made by computing the far-field noise contributions of these two components.

The paper is organized as follows. After the introduction, the underlying improved elements of the LBM flow solver, as well as the analysis techniques, are described in Section II. In Section III, details of the nozzle configurations and computational setup are reported. Next, in Section IV, the results are validated against experimental material for one single jet condition. A detailed comparison for the different setpoints follow in Section V. The physical insight of a heated core case (setpoint 46) is continued in Section VI, where the wavelet decomposition technique and azimuthal FW-H computations are used to shed some light on the source generation mechanisms. Conclusions and further outlook are finally reported in Section VII.

II. PowerFLOW physics and analysis techniques

The numerical solver, which is based on the Lattice Boltzmann Method (LBM) with a wall modeled Very Large Eddy Simulation (VLES) model for turbulence,[18–21] has been extensively discussed and successfully used for a wide range of industrial applications.

Earlier versions of PowerFLOW for subsonic and transonic applications involved solving the entropy equation using a Finite Difference Method (FDM).[22] This FDM however had two main sources of numerical errors: 1) a certain dependency of the solution on the grid orientation observed as a lost of symmetry in the azimuthal direction of second order moments (standard deviation) and higher, and 2) pressure disturbance and conservation issues across interfaces between Variable Resolution (VR) regions of the computational

grid. Also, FDM raised difficulties in applying boundary conditions for complex geometries. In order to overcome these limitations and sources of numerical errors, an LBM based entropy solver has been recently developed by introducing an additional set of distribution functions.

The new entropy solver developed is similar to the scalar solver developed by Zhang *et al.*[23] Most LBM based scalar solvers available in the open literature uses total scalar (i.e. scalar multiplied by mass) as its second distribution. In PowerFLOW's unique approach,[24] the second distribution function is based on a specific scalar quantity and therefore, the total conservation is ensured by multiplying the second scalar distribution with the fluid particle distribution. This approach offers a wide stability range and can maintain a constant scalar field under many varying flow conditions. Recently also further stability enhancement is made for high Mach number flows by modifying the collision operator to one based on PowerFLOW's unique Galilean invariant form.[25]

Due to the unique properties of PowerFLOW, which is intrinsically unsteady and compressible, the acoustic pressure field can be extracted directly from the computational domain. In addition, in this work, the far-field noise is obtained by using a FW-H analogy, where the sampling surface is fitted to a permeable surface surrounding the turbulent regime. The employed FW-H approach is based on a forward-time solution[26] of Farassat's formulation 1A,[27] and available in Exa's post-processing software PowerACOUSTICS.

In addition to the standard time-domain FW-H approach available in PowerACOUSTICS, a frequency-domain FW-H model is also used in this work. It is based on the formulation proposed by Lockard,[16] but extended to a three-dimensional flow field. This formulation is theoretically consistent with a time-domain formulation, but it implies Fourier transforms of the FW-H source terms instead of the transient far-field signals, as well as a different spectral averaging process, which can lead to different results. It is therefore useful to compare the two far-field extrapolations to get an indication about the numerical uncertainty related to the acoustic analogy integral. Another interesting aspect of the frequency-domain FW-H is its usage in combination with an azimuthal Fourier transform of the FW-H source terms, as a way to investigate the acoustic efficiency of the different azimuthal flow perturbation modes.

Since the pioneering experimental observations made by Mollo-Christensen,[28] the existence of coherent hydrodynamic structures in the shear layer of a jet and their connection with the radiation of sound have been the topic of several studies. The review article by Jordan & Colonius[29] provides evidence of connection between the time evolution of these coherent hydrodynamic structures and the far-field noise in different regimes of the convection phase velocity with respect to the ambient speed of sound (acoustic Mach number). Subsonic convection is associated with evanescent waves (pseudo sound), whereas supersonic convection generates Mach waves[30] that affect the downstream radiation. The dual hydrodynamic and acoustic nature of the near-field of a jet has been investigated in the past.[31,32] Recently, a wavelet-based decomposition technique has been proposed by Mancinelli *et al,*[17] which is based on recursive de-noising procedure (WT3). The same technique is applied in the current work to separate the coherent and chaotic flow motion in the near-field of a heated core jet, characterised by the presence of structures with a supersonic phase velocity, thus radiating Mach waves. As an original contribution of the present work the FW-H analogy is applied to the coherent and chaotic contributions on the permeable surface encapsulating the jet plume separately, providing further physical insight into the sound generation mechanisms in the far-field.

III. Nozzle geometry and computational setup

The nozzle geometry under consideration is the 2-inch diameter ($D_j = 0.0508$ m) convergent SMC000 nozzle, see Fig. 1. The primary convergent nozzle assembly has a 6-inch diameter inlet, followed by a strong geometry contraction to a 5° taper near the nozzle exit. This is a well established benchmark case for jet flow and acoustics, and it has been extensively studied by experimental works performed before in the Small Hot Jet Acoustic Rig (SHJAR) at the Aeroacoustic Propulsion Laboratory at NASA Glenn.[13,14]

By including the physical nozzle in the simulation domain, it was possible to avoid the usage of boundary conditions to reproduce the time-average and fluctuating part of the jet at the exhaust plane. The centerline of the nozzle is set along the x-axis, and the computational domain has been partitioned into 13 VR regions, as illustrated in Fig. 2. This is done in order to locally resolve the the shear layer flow, while keeping the computational cost to a minimum. The methods is similar to grid stretching techniques often applied in other computational codes. Each grid cell is further denoted as a voxel. The voxel size between each successive VR region differs by a factor of two. On average, for the medium resolution (resolution for which results in this paper are generally reported), a total of 625 million voxels has been used. VR10 is used

American Institute of Aeronautics and Astronautics
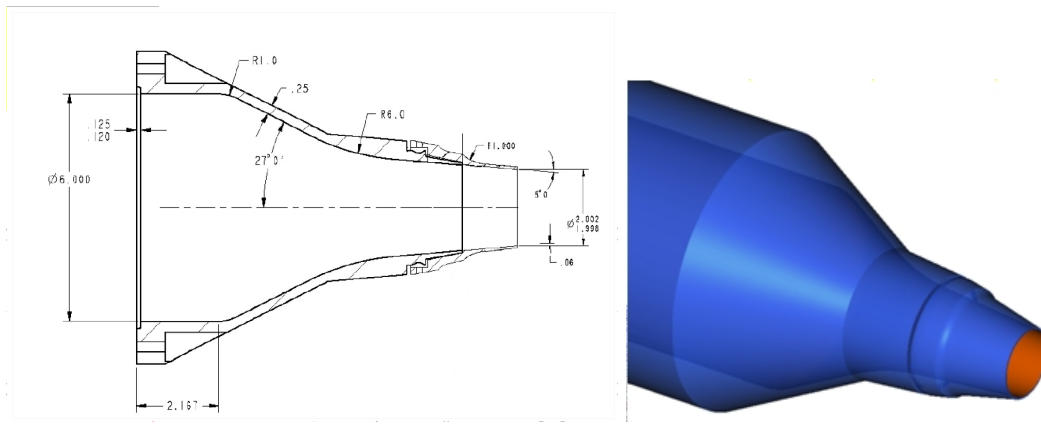
Figure 1. Overview of the nozzle geometry.

as reference resolution layer, with 64 voxels along the nozzle core diameter. This results in a finest voxel size of 0.0992 mm in VR13, corresponding to a local y^+ value at the nozzle exit of 15. Due to the explicit time-stepping characteristics of the LBM scheme, time-steps are increased with voxel size in factors of two as well. Larger voxels will therefore not be evaluated every time step. The equivalent number of voxels updated at every time step can be therefore defined, say Fine Equivalent Voxels (FEV), which are 160 million for this study.
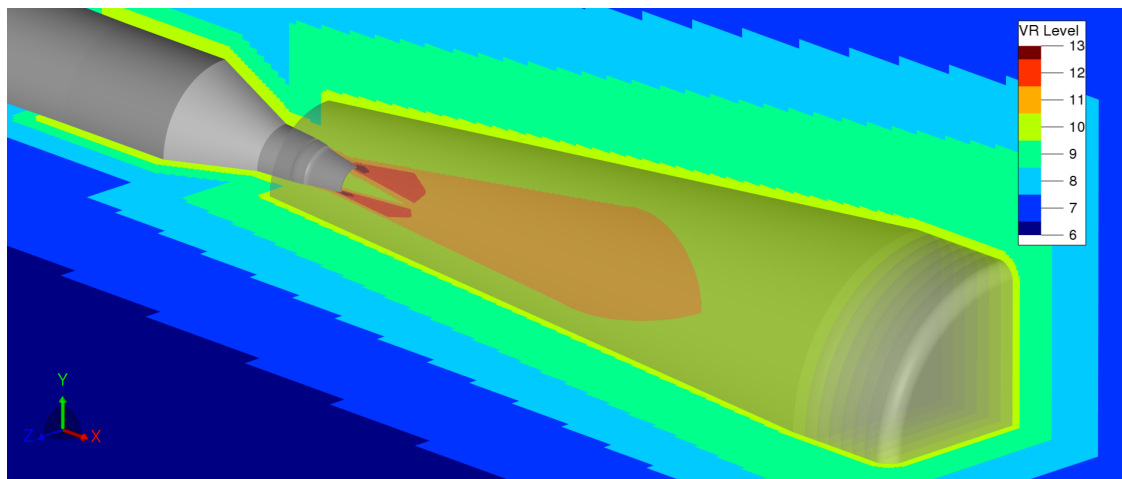
Figure 2. Details of the simulation setup: geometry, VR's and FW-H permeable surface.

Non-reflecting free-field boundary conditions and sponge zones are used to prevent the inward reflection of acoustic waves. The sponges are characterized by an exponential increase of the damping parameter from a distance of 75 m from the nozzle exit. At the nozzle inlet, total pressure and total temperature inlet conditions are set according to the simulation matrix in Tab. 1. Three conditions are simulated: 1) Low-subsonic and unheated core (SP03), 2) High-subsonic and unheated core (SP07) and 3) High-subsonic and heated core (SP46). Far-field acoustics are extracted using the FW-H analogy using a permeable surface surrounding the plume. A truncated conical surface of axial extension equal to 24 nozzle diameters is used (see Fig. 2). The angular opening of the cone is expected to reproduce the jet spreading for different Mach numbers and temperature ratios, following Witze's formula.[33] In order to have a better acoustic prediction at shallow radiation angles, where Mach wave radiation is expected to dominate for the high-subsonic cases, the downstream termination of the FW-H surface is equipped with five staggered cups that, by averaging the far-field noise signals, would allow filtering the signature of the vortical perturbations passing through the integration surface.[5,34]

After an initial convergence stage towards a stable transient solution, simulations are performed for a physical time of 0.07 s. A total number of 45 kCPUh are required (distributed over 700 cores). Spectral

American Institute of Aeronautics and Astronautics

	SP03	SP07	SP46
Ma	0.5	0.902	0.901
T/T_∞	0.955	0.842	2.702

analyses are subsequently performed by performing 30 Welch averages with about 50 % overlap. The overlap coefficient is trimmed case by case in order to exploit the whole duration of the transient solution and guarantee a minimum frequency of 200 Hz.

IV. Validation

Validation of the prescribed methodology is based on the high subsonic, heated core setpoint (SP46), the most challengin out of the list of three. Its characheristic quantities are found back in Tab. 1, while details about the different analyzed grids are depicted in Tab. 2. Both the aerodynamic centerline flow extraction and far-field noise levels are compared for different grids.

Table 2. Grid information matrix and computational cost for SP46.

	Voxel size	Voxels	FEV	kCPUh
Very coarse	32	110	30	5
Coarse	45	250	65	15
Medium	64	625	160	45
Fine	90	1560	380	140

IV.A. Flow field

The time-average (mean) and standard deviation (fluctuating) streamwise velocity components extracted along the jet centerline over a distance of 20 nozzle diameters from the nozzle exit are plotted in Fig. 3. The standard deviation of the streamwise velocity is computed by making an isotropic turbulence assumption for the small unresolved turbulence scale, thus adding $2K/3$ to the resolved fluctuation levels, K being the modeled turbulence kinetic energy. For the very coarse and coarse grid, the jet mixing is delayed and fluctuations are underpredicted with respect to the measurements.[14] A convergence to the experimental results is found when refining further, showing excellent agreement for medium and fine resolution grids. In particular, the slope of the fluctuation level is in fairly good agreement with the measurements, and this reveals that the correct shear layer instability mechanisms are properly simulated by the numerical solution.
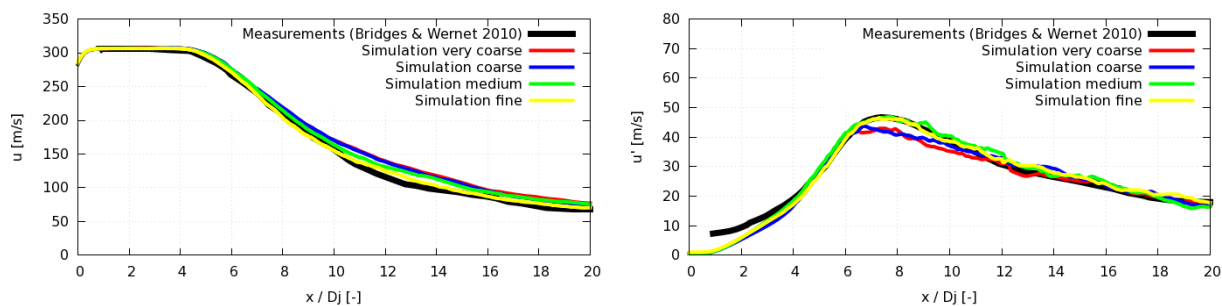
Figure 3. Setpoint 46: Mean and fluctuating streamline velocity along the centerline

Mean and fluctuating streamwise velocities are also extracted along the nozzle lipline and plotted in Fig. 4. Good agreements with measurements are found for locations larger than two jet core diameters downstream the lipline. As stated in Ref.,[14] the region of the lipline close to the nozzle is affected by large experimental uncertainties. Nevertheless, the current results in this paper are in better agreement with

American Institute of Aeronautics and Astronautics

experiments compared to other recent results obtained with other (hybrid RANS)-LES models.[5,35–42]

Figure 4. Setpoint 46: Mean and fluctuating streamline velocity along the lipline.

IV.B. Acoustics

Near-field acoustic wave radiation can be visualized by means of dilatation fields. A snapshot of the time derivative of the pressure in Fig. 5 shows downstream radiation of Mach waves coming off from large-scale fluctuations in the shear layer.
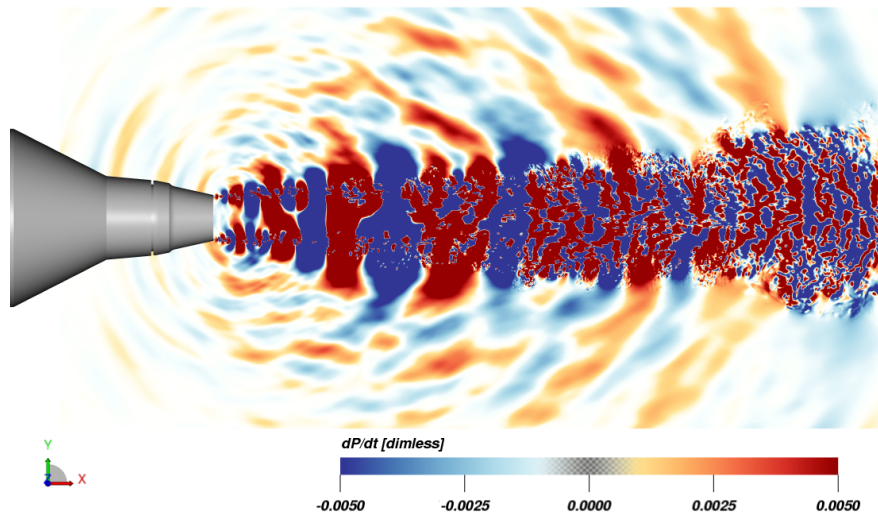
Figure 5. Setpoint 46: Snapshot of dilatation field.

The effect of mesh resolution on the far-field results is illustrated by $1/3-$octave acoustic spectra at different angular positions, as well as with the overall sound pressure levels (OASPL) directivity. Noise spectra at four different angular locations are considered in Fig. 6; from $75°$, upstream the nozzle exit, to $165°$, a downstream shallow angle. A consistent converging behavior can be observed at all angles, with a clear increase of the cut-off frequency due to a more accurate prediction of the acoustic propagation from the sources in the plume to the FW-H integration surface. The shape of the acoustic spectra are quite well predicted, also by a very-coarse grid. This reveals the robustness of the computational setup and the absence of spurious noise sources. The OASPL directivity plot in Fig. 7 exhibit a clear grid-independent behavior, with maximum deviation from the measurements of about $1\,\mathrm{dB}$. Overall, it can be confirmed that these results are in better agreement with experiments compared to other recent results obtained with other (hybrid RANS)-LES models.[5,35–42]

A spectral representation of the noise directivity is shown in Fig. 8 for the medium resolution, where the typical Mach wave downstream radiation pattern can be observed. Due to lower statistical convergence, the numerical solution is not as smooth as the experimental one. Azimuthal averaging could be a solution here, which will be investigated in a next study. However, beside this, an overall good comparison can be be observed between simulation and experiment.

American Institute of Aeronautics and Astronautics
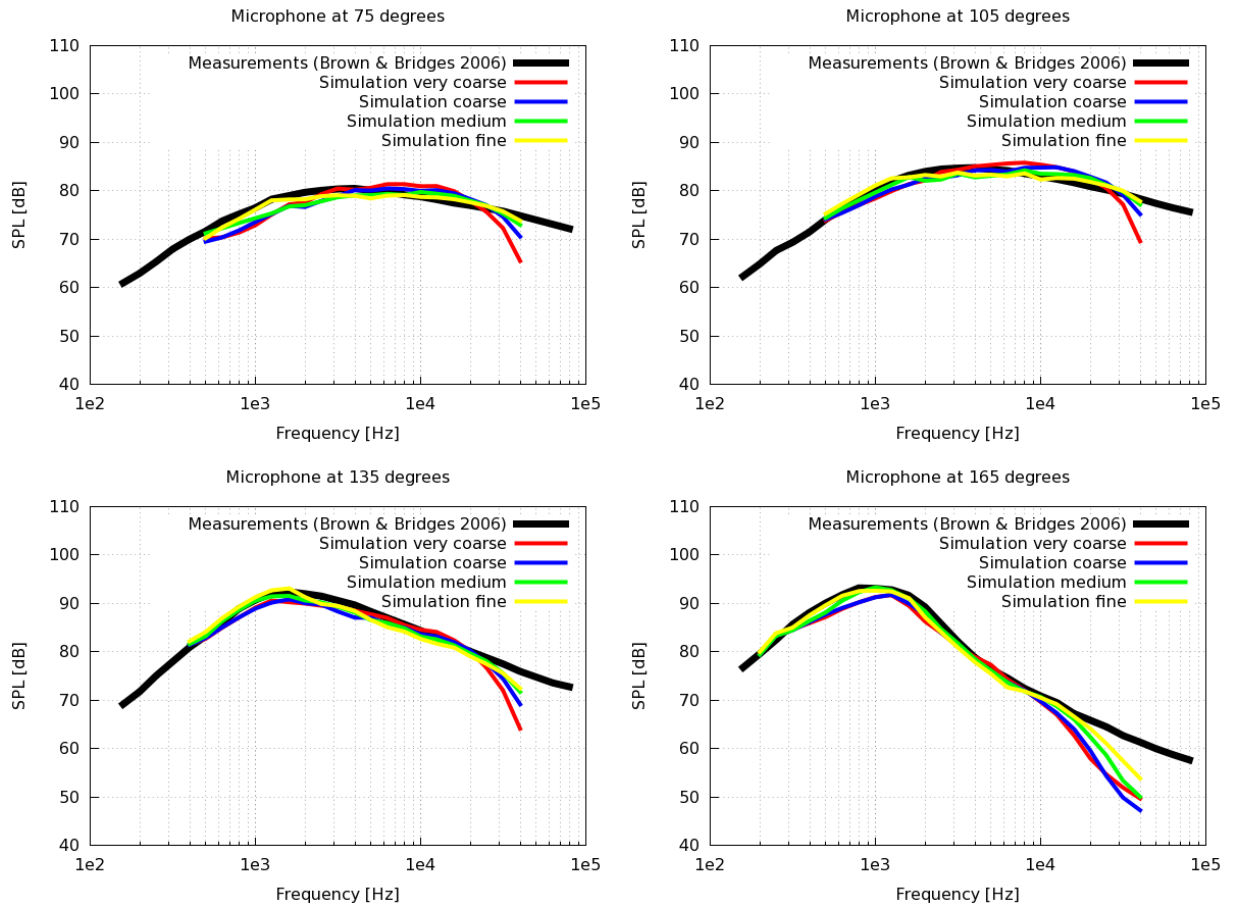
Figure 6. Setpoint 46: Far-field noise levels at various microphone locations.
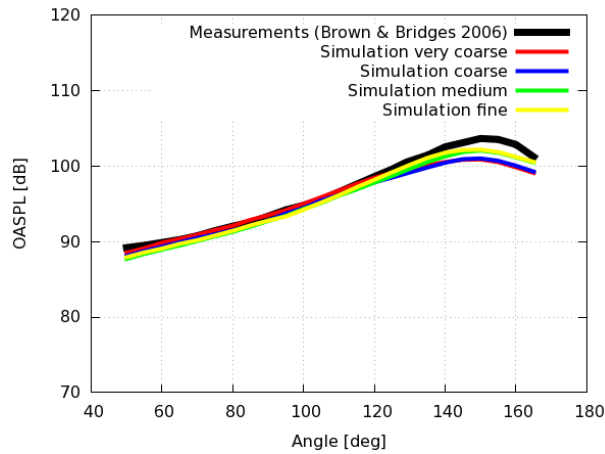
Figure 7. Setpoint 46: OASPL directivity pattern.

V.   Setpoint comparisons

This section contains a comparison between different setpoints and the corresponding experimental data. Having achieved grid-independent acoustic results with a medium resolution grid, this resolution level is used to carry out this comparative study.

American Institute of Aeronautics and Astronautics
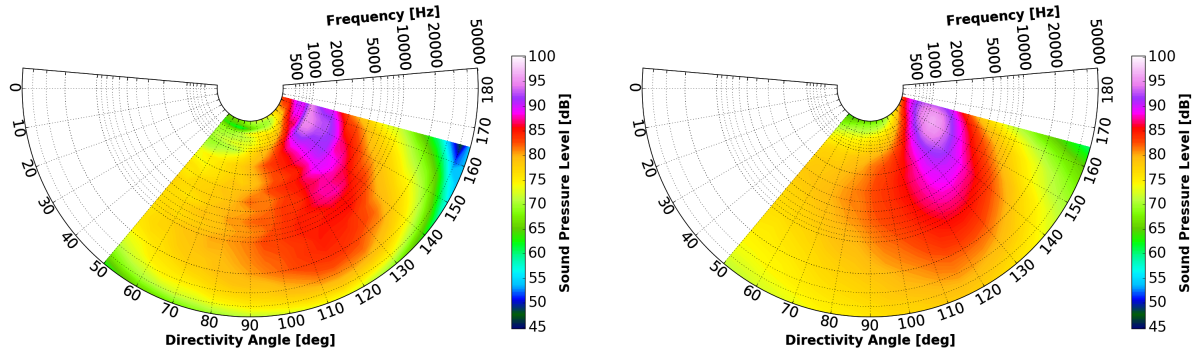
Figure 8. Setpoint 46: Directivity analysis of (left) numerical data and (right) experimental data. FIne resolution results.

V.A.   Flow field

Figs. 9,   10 and 11 are used to qualitatively analyze the jet plume variation. What can be observed is the increase in Mach number and standard deviation for the high-subsonic cases (cold SP07 & hot SP46). Furthermore, due to the high temperature ratio of SP46, the actual Mach number is significantly smaller than the acoustic Mach number. This makes it possible to simulate this jet condition by using the high-subsonic solver, whereas the cold jet is approaching the limitation of the high-subsonic LBM implementation in PowerFLOW ($M < 0.95$).   It is interesting to notice the the fluctuation velocity contours exhibit some
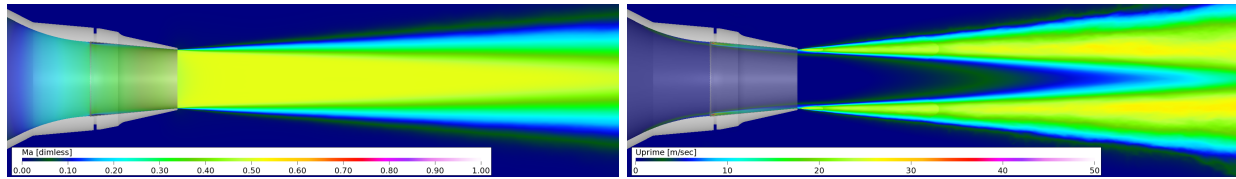
Figure 9. Setpoint 03: Mean Mach number (left) and fluctuation velocity (right).
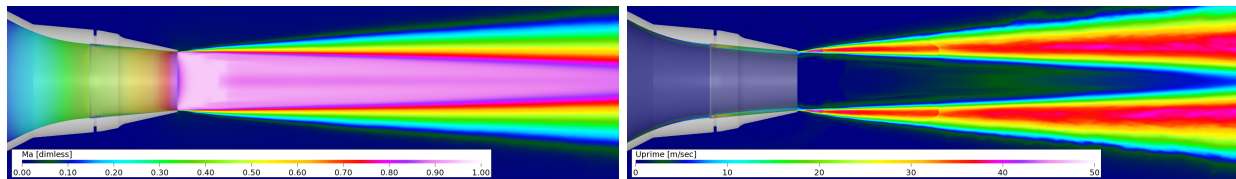
Figure 10. Setpoint 07: Mean Mach number (left) and fluctuation velocity (right).
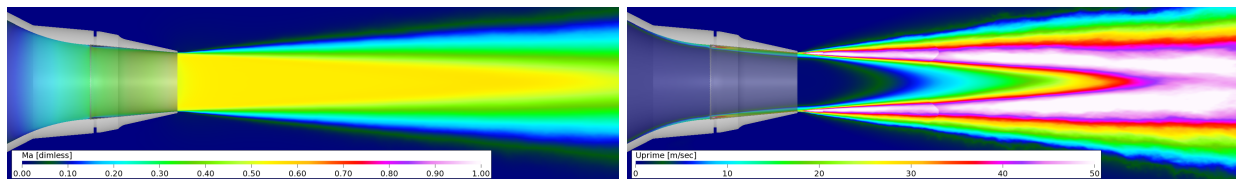
Figure 11. Setpoint 46: Mean Mach number (left) and fluctuation velocity (right).

small discontinuities in the shear layer. These are located at VR interfaces. The effect is however very local, and this denotes that the LBM implementation in PowerFLOW, and in particular the new LB solver of the entropy equation, are weakly sensitive to changes of the grid resolution. This is a crucial aspect in non-isothermal applications, and a clear advantage of the present LB entropy solver with respect to the previous FDM implementation.

American Institute of Aeronautics and Astronautics

V.B.   Acoustics

In order to illustrate the variation of noise emission between the three different setpoints, four microphone locations are considered (Fig. 12), as well as the OASPL (Fig. 13). Numerical results are compared against data from Brown & Bridges.[13] Multiple observations can be made. Firstly, the numerically obtained spectra are in close agreement with the experimental data-set, for different setpoints and different microphone angular positions.

There seems to exist a trend between both cold setpoints (SP03 & SP07). Both solutions show similar spectra and directivity pattern, with the highest amplitude found at shallow angles (> 135 deg) moving from $2,000$ Hz at 135 deg to $1,000$ Hz at 165 deg. The difference between the two spectral levels is fairly constant and measured to be about $21\,\mathrm{dB}$, close to the acoustic variation of a quadrupole source from two different jet exhaust velocities: $80 \log_{10}(M_{\mathrm{SP07}}/M_{\mathrm{SP03}}) = 80 \log_{10}(0.902/0.5) = 20.5\,\mathrm{dB}$.
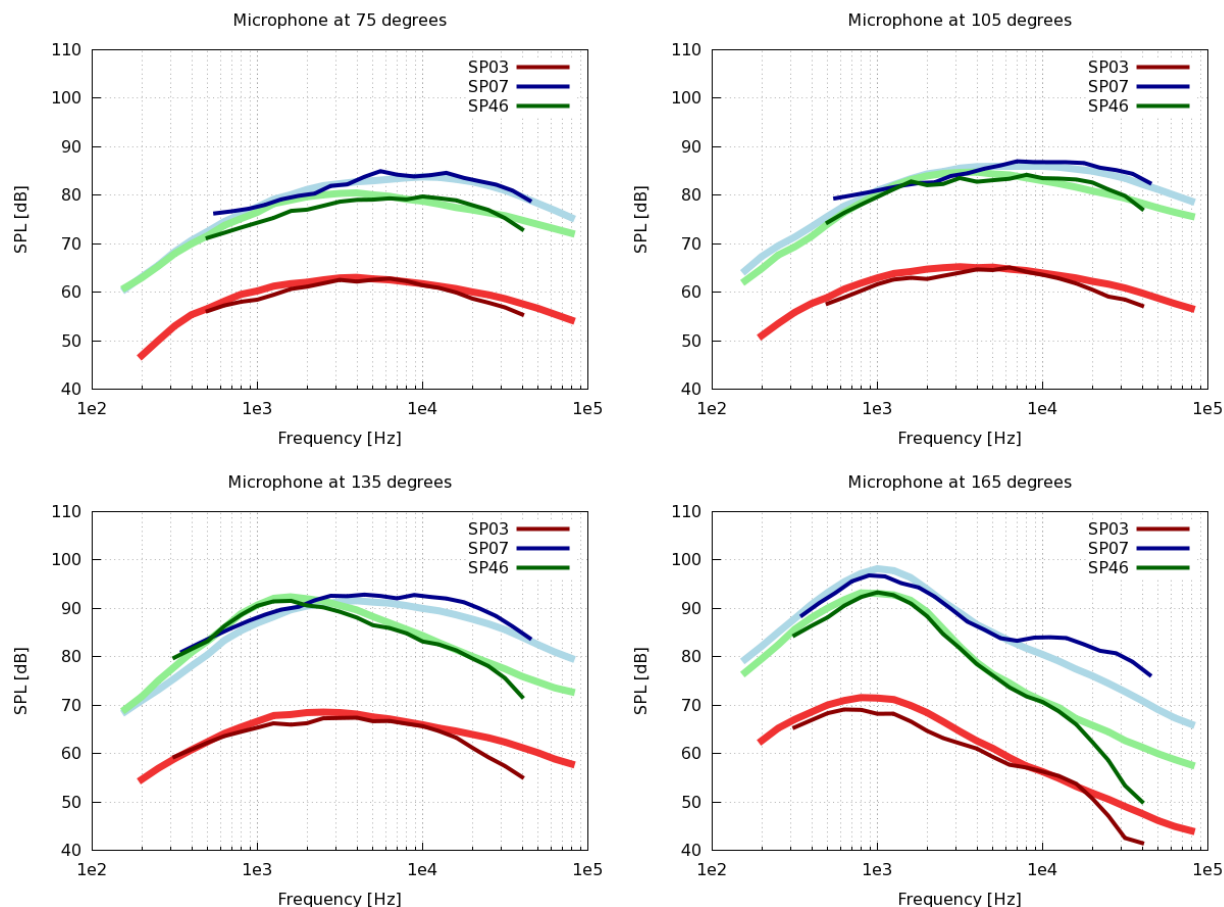
Figure 12.   Comparison of setpoints: Far-field noise levels for various microphone locations. The light, thick lines corresponds to the experimental dataset from Brown & Bridges.[13]

The hot jet setpoint exhibits a different spectral trend compared to the cold cases, by having a peak in amplitude at lower frequency for centered angles (around $90°$). Furthermore, at the shallow angles, a slight reduction of noise is observed between $5,000$-$10,000$ Hz. This is in line with the experimental data.

A discrepancy in the spectra is found for the high-subsonic cold setpoint SP07 around $10,000$ Hz. As previously pointed out, the local velocity of this setpoint exceeds the Mach number limitation of the subsonic solver, and therefore high-frequency numerical fluctuations are generated which will affect the acoustic spectra. A future study will demonstrate that this error can be reduced by using a transonic formulation of PowerFLOW LBM solver.

American Institute of Aeronautics and Astronautics
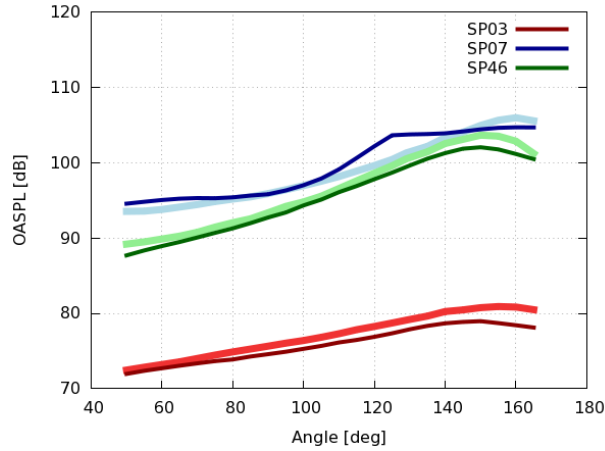
Figure 13. Comparison of setpoints: Overall far-field noise levels for all microphones. The light, thick lines corresponds to the experimental dataset from Brown & Bridges.[13]

VI.   Physical insight

In order to gain some physical insight into the sound generation mechanisms, detailed analyses are carried out for the heated core setpoint 46. First, a wavelet decomposition technique is used to separate the coherent from the chaotic fluctuations in the plume of the jet. The decomposition is initially applied to the pressure field acquired on a meridional plane. Then, the wavelet decomposition is applied to the complete set of flow variables on the FW-H permeable surface. The coherent and chaotic inverse-wavelet transient solutions are further used to compute the noise in the far-field. Finally, use of a frequency domain FW-H solver is made in order to investigate the relative importance of different azimuthal modes in the plume of the jet.

VI.A.   Near-field wavelet decomposition

The jet shear layer is investigated by means of a wavelet decomposition WT3,[17] as described in Section II. A default set of wavelet (Daubechies-12 type) and a unitary threshold coefficient were used for the decomposition of pressure. The same threshold was used to separate all the flow variables on the FW-H permeable surface. This is however not a guarantee that the two sets of segregated flow variables are independently a solution of the flow governing equations. Further investigations are necessary to clarify this point.

Before applying the wavelet decomposition on a field solution, pressure signals extracted at locations close to the shear-layer interface are analyzed. The results are reported in Fig. 14 for one single probe, while Fig. 15 reports the variation in hydrodynamic and acoustic contribution along the shear layer line.

Fig. 14 depicts two different spectra; a more broadband acoustic spectrum and a more low-mid frequency range hydrodynamic spectrum. It can therefore be clearly seen that the total spectra is a combination of two different spectral energies, resulting into different spectrum energy decays. It furthermore shows a a cross-over frequency of $St_D = fD/u_\infty \approx 0.3$, where the acoustic contribution becomes more dominant than its hydrodynamic counterpart. Below $St_D < 0.3$, a difference up to 10 dB is observed between both contributions. These typical numbers are in very close agreement with the study from Mancinelli *et al.*[17]

The axial evolution of the hydrodynamic and acoustic pressure spectra are shown in Fig. 15. For the hydrodynamic contribution, a clear hump is visible around $St_D = 0.2$. This energetic hump moves to lower frequencies as the axial distance from the nozzle is increasing, which can be connected to the development of larger structures downstream the jet plume. The opposite is true for the acoustic contribution; its energy level decreases when moving downstream the jet. Such trends are in agreement with the results from Grizzi & Camussi[43] and Mancinelli *et al.*[17] A further study will try to focus on capturing Mach number dependencies.

To highlight the variation between both contribution in a more qualitative fashion, a dB pressure map of the field solution is depicted for two key frequencies. The results are plotted in Fig .16 & 17 for 1,000 and 5,000 Hz respectively, resulting in in Strouhal numbers of 0.3 and 1.5. Multiple observations can be made; at low Strouhal numbers, inside the jet plume, the coherent (hydrodynamic) part of the pressure dominates over the chaotic (acoustic) part. The higher Strouhal numbers on the other hand, have a very
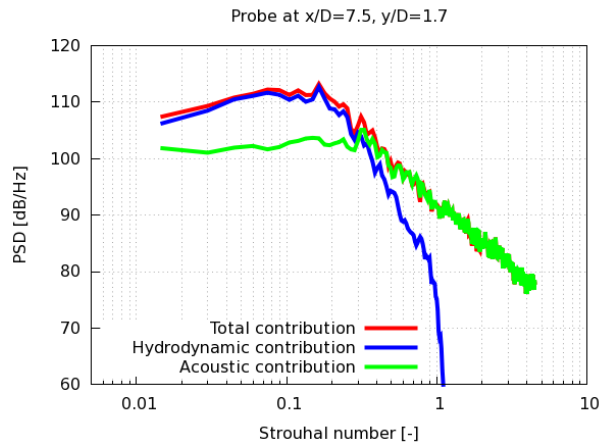
Figure 14. Setpoint 46: Near-field wavelet decomposition close to the shear-layer boundary.
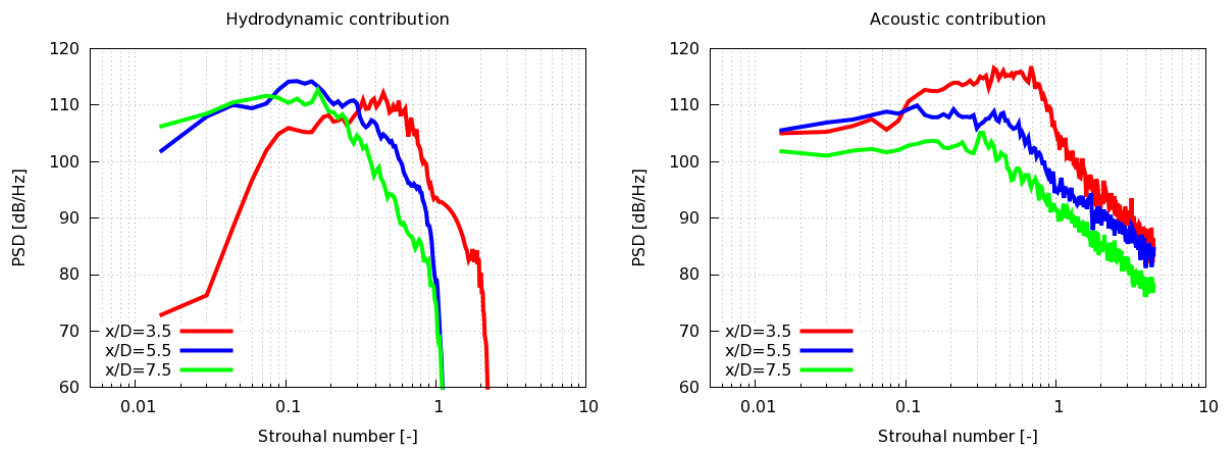
Figure 15. Setpoint 46: Near-field wavelet decomposition at different downstream locations of the jet close to the shear-layer boundary for both the hydrodynamic (left) and acoustic (right) contribution.

low hydrodynamic pressure amplitude compared to its acoustic counterpart. This is in line with the graphs presented earlier. Finally, it is interesting to note that the acoustic contribution at a low Strouhal number is more or less depicted as a Mach radiation wave (Fig. 16, right).
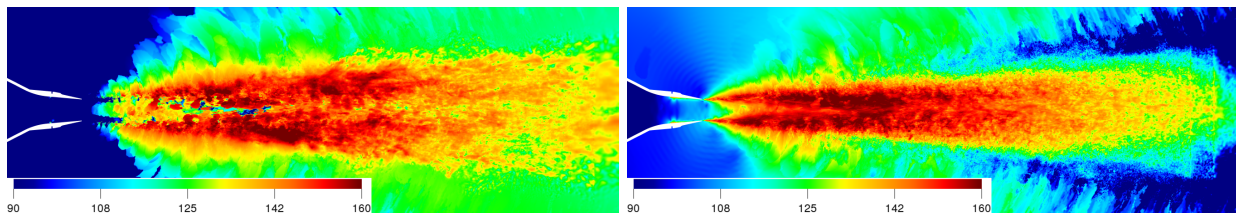
Figure 16. Setpoint 46: 1,000 Hz dB map of (left) hydrodynamic & (right) acoustic part of the pressure after wavelet decomposition.

VI.B.   Far-field wavelet decomposition

In the acoustic far-field, a similar wavelet decomposition is attempted using the process described in previous section. The difference however is that in this particular case, the decomposition is applied on both velocity, pressure and density obtained from the sampled permeable FW-H surface surrounding the entire jet plume. Using a FW-H calculation, far-field pressures are obtained, seen in Fig. 18. Notice that due to the large computational cost of performing a full wavelet decomposition on a permeable surface, only one inverse
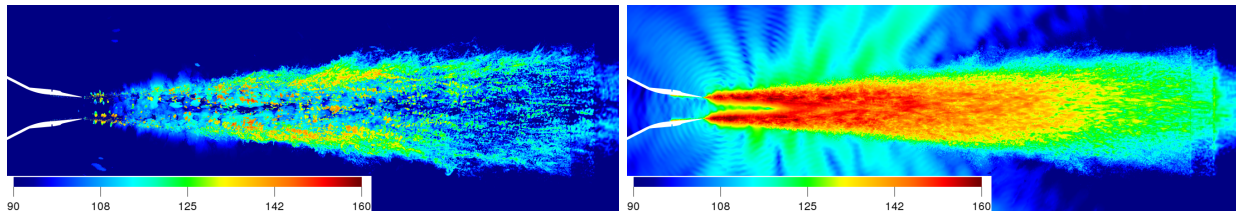
Figure 17. Setpoint 46: 5,000 Hz dB map of (left) hydrodynamic & (right) acoustic part of the pressure after wavelet decomposition.

wavelet over a spectral window was saved during this process. This explains the fact the the spectra are not as smooth as the ones presented before.

Interestingly, it can be observed that the hydrodynamic contribution is dominant over all frequencies while the acoustic contribution nearly exceeds the 60 dB. As the permeable FW-H surface is still located in the near hydrodynamic field, the result is as expected. Further research is required though, as the results were obtained with the assumption that both velocity, density and temperature are decomposed with the same default set of wavelets and threshold.
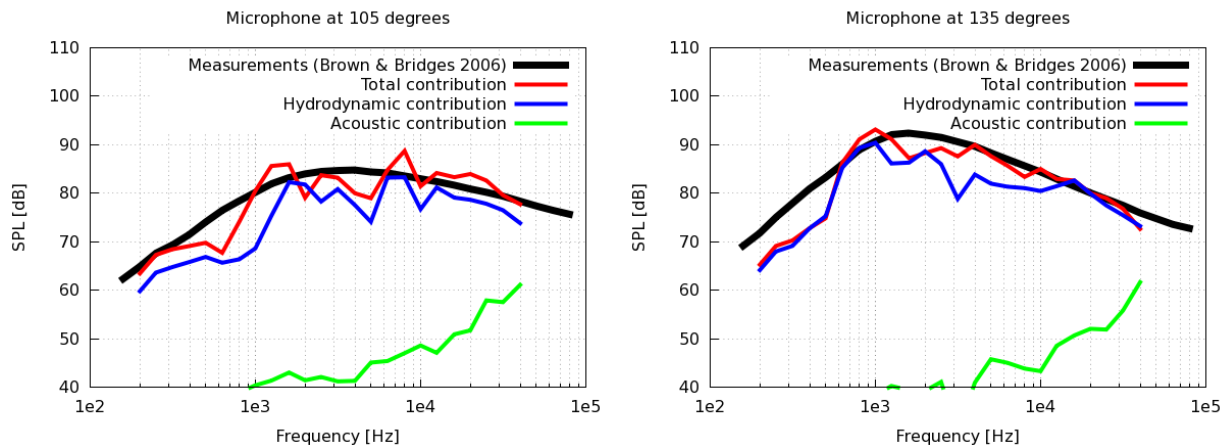
Figure 18. Setpoint 46: Far-field noise levels obtained from the wavelet decomposition, separating the hydrodynamic and acoustic pressure.

An interesting outcome though of this analysis is that the acoustic far-field can be completely rebuilt from a reduced order model of the near field, based on about 5% of the original information corresponding to the relative number of wavelet terms in the coherent part. This observation can have important implications in the development of noise control strategies and further physical understanding.

VI.C. Far-field azimuthal analysis

Another decomposition performed is the split of the far-field signal into different azimuthal modes, performed by applying a FW-H calculation in frequency domain. Details of the methodology can be found in Section II.

Before analyzing the various modes obtained from the FW-H solution in frequency domain, it is crucial to check the accuracy of the implemented frequency domain solver. Therefore, in Fig. 19 a comparison between the time domain solver (original implementation in PowerACOUSTICS) is compared against the frequency domain solver. The overall agreement of the two depicted microphone positions is excellent; differences within a 1 dB range are observed.

The first 5 azimuthal modes for four microphone positions, as well as OASPL are illustrated in Fig. 20 & Fig. 21 respectively. Multiple observations can be made. First of all, for all radial directions, the most dominant plane mode found is mode 0. For sharp and moderate angles (< 105 deg) mode 0, 1 & 2 are behaving similarly; with similar trends for similar amplitudes. A summation of these modes will almost represent the full, experimental spectra.

For the more shallow angles (> 105 deg), a larger variation between the different modes start exist. This is pronounced at a shallow angle of 165 deg, where mode 0 till 4 vary between trend and amplitude. For

American Institute of Aeronautics and Astronautics
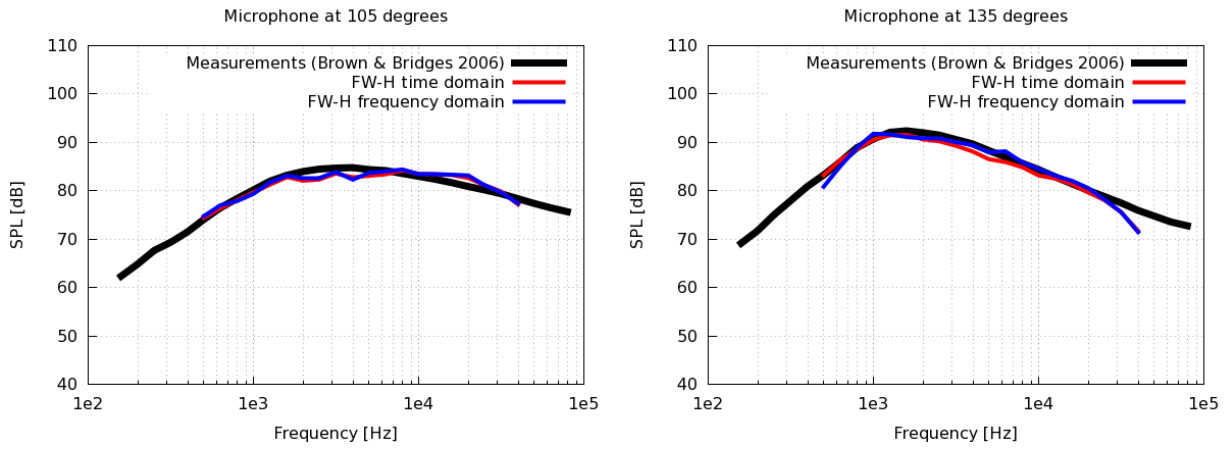
Figure 19. Setpoint 46: Far-field noise levels obtained from both the FW-H time and frequency domain implementation.
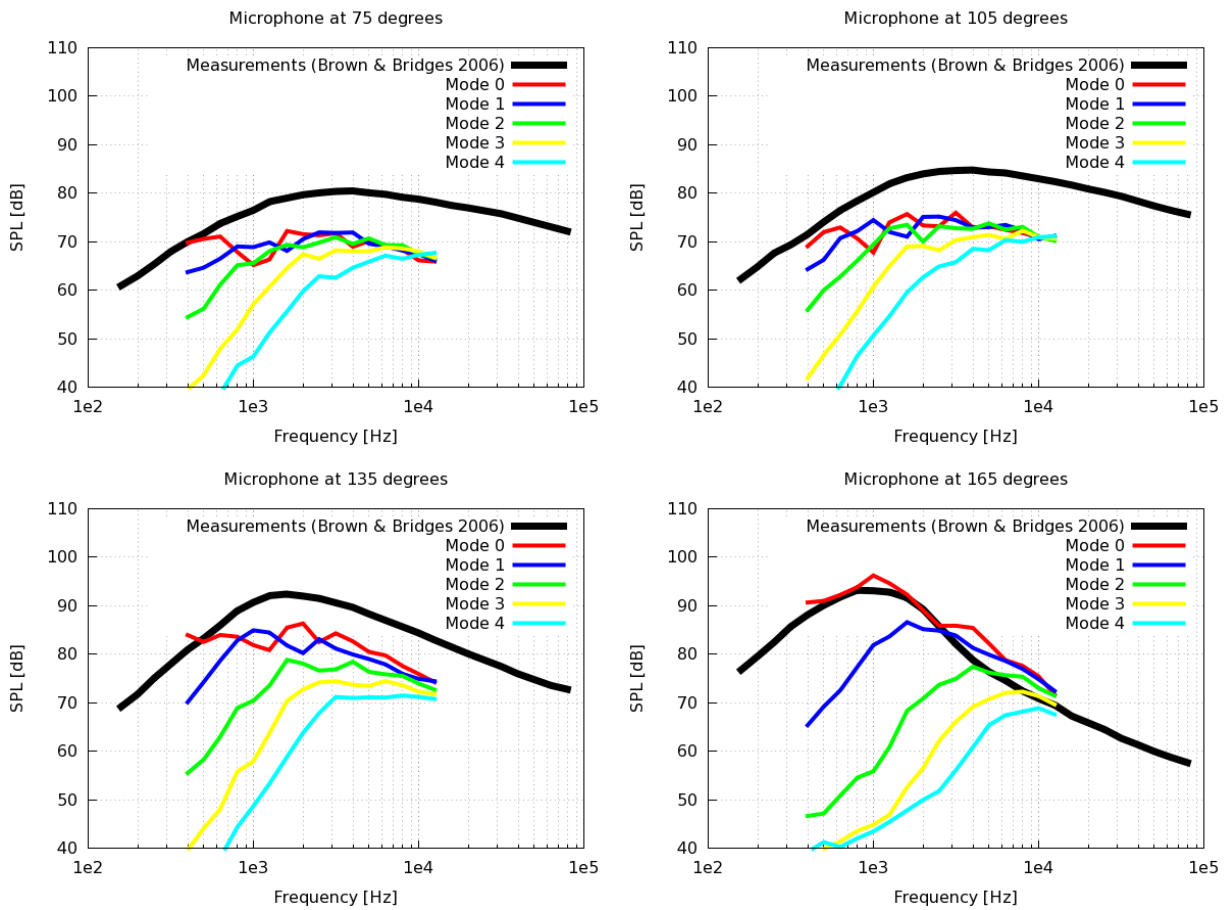
Figure 20. Setpoint 46: Far-field noise levels obtained with modal information.

these angles, mode 0 almost represent the full energy spectrum. This interesting observation suggests that the various modes are convected differently, resulting in a distinctive directivity pattern.

To confirm this peculiar behavior, Fig. 21 presents the OASPL for all microhones. Noteworthy is the diversification of the amplitude between the modes; growing with increasing angle.

American Institute of Aeronautics and Astronautics
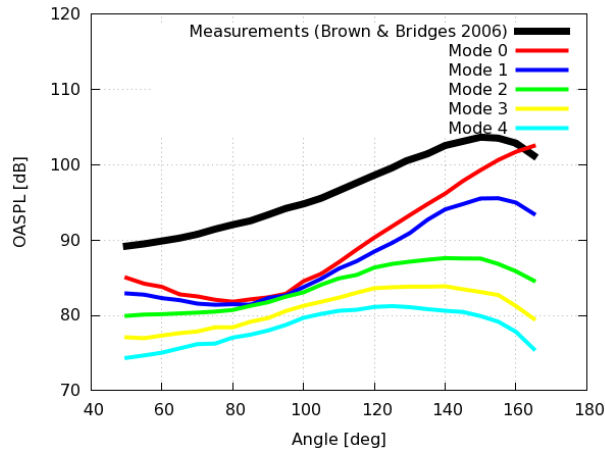
Figure 21. Setpoint 46: Overall far-field noise levels for all microphones with modal information.

VII. Conclusion

PowerFLOW, the numerical solver based on the Lattice Boltzmann Method (LBM) with a wall modeled Very Large Eddy Simulation (VLES) model for turbulence, was used to simulate the unsteady jet flow exhausting from a single axi-symmetric nozzle, as well as the associated noise spectra and directivity. The jet exit Mach number and temperature ratio were set according to the various setpoints from the NASA SMC000 experimental campaign. Both isothermal and heated core flows were considered. The far-field noise was computed through a Ffowcs-Williams and Hawkings (FW-H) analogy applied to a fluid surface encompassing the jet plume. Both time- and frequency-domain formulations were used, the latter in combination with an azimuthal Fourier transform of the linear source terms to analyze the contribution of the different azimuthal components.

A resolution study was first carried out for both aerodynamic and acoustic results of setpoint 46. The near- and far-field results confirmed that the underlying flow features and noise mechanisms were fully represented by the numerical solution. Furthermore a comparison between the different setpoints were showcased, again with good resemblance against experimental spectra.

A physical insight into the acoustic source mechanisms was further conducted. A wavelet decomposition was first applied to the turbulent near-field flow to separate the coherent flow motion, usually attributed to the hydrodynamic fluctuations, and the chaotic perturbations, which have a more dominant acoustic character. The results indicated a cross-over frequency from which the acoustic perturbations dominate with respect to the hydrodynamic perturbations. The wavelet decomposition was also applied to the far-field, in combination with a FW-H solver, showing the majority of the contribution coming from the hydrodynamic pressure. Further study is required to corroborate some of the findings.

Finally, the time- and frequency-domain FW-H formulations were both compared, before analyzing the different azimuthal flow perturbation modes. It was found that at sharp and moderate angles, the modes behave similarly. However, when analyzing shallow angles, the results disparate, indicating strong convection effect along the various modes.

References

[1]Bridges, J. E., Podboy, G. G., and Brown, C. A., "Testing Installed Propulsion For Shielded Exhaust Configurations," *AIAA Paper 2016-3042*, 2016.

[2]Hazir, A. and Casalino, D., "Lattice Boltzmann Based Aeroacoustic Simulation of Turbofan Noise Installation Effects," *Proceedings of the 23rd International Congress on Sound and Vibration, Athens, Greece*, 2016.

[3]Bodony, D. J. and Lele, S. K., "Current Status of Jet Noise Predictions Using Large-Eddy Simulation," *AIAA Journal*, Vol. 46, No. 2, 2008, pp. 364–380.

[4]Brès, G. A., Ham, F. E., Nichols, J. W., and Lele, S. K., "Unstructured Large-Eddy Simulations of Supersonic Jets," *AIAA Journal*, Vol. 55, No. 4, 2017, pp. 1164–1184.

[5]Spalart, P. R., Shur, M. L., Strelets, M. K., and Travin, A. K., "Jet Noise Computation Based on Enhanced DES

American Institute of Aeronautics and Astronautics

Formulations Accelerating the RANS-to-LES Transition in Free Shear Layers," *International Journal of Aeroacoustics*, Vol. 15, No. 6–7, 2016, pp. 595–613.

[6] Shur, M., Strelets, M., Travin, A., Spalart, P. R., and Suzuki, T., "Unsteady Simulations of a Fan/Outlet-Guide-Vane System. Part 1: Aerodynamics and Turbulence," *AIAA Paper 2017-3875*, 2017.

[7] Casalino, D., Ribeiro, A. F. P., Fares, E., and Nölting, S., "Lattice-Boltzmann Aeroacoustic Analysis of the LAGOON Landing Gear Configuration," *AIAA Journal*, Vol. 52, No. 6, 2014, pp. 1232–1248.

[8] Casalino, D., Ribeiro, A. F. P., and Fares, E., "Facing Rim Cavities Fluctuation Modes," *Journal of Sound and Vibration*, Vol. 333, No. 13, 2014, pp. 2812–2830.

[9] Casalino, D., Hazir, A., and Mann, A., "Turbofan Broadband Noise Prediction using the Lattice Boltzmann Method," *AIAA Journal*, Vol. 56, No. 2, 2018.

[10] Khorrami, M. R., Fares, E., and Casalino, D., "Towards Full Aircraft Airframe Noise Prediction: Lattice Boltzmann Simulations," *AIAA Paper 2014-2481*, June 2014.

[11] Fares, E., Casalino, D., and Khorrami, M., "Evaluation of Airframe Noise Reduction Concepts via Simulations Using a Lattice Boltzmann Approach," *AIAA Paper 2015-2988*, 2015.

[12] Casalino, D., Hazir, A., and Mann, A., "Turbofan Broadband Noise Prediction using the Lattice Boltzmann Method," *AIAA Paper 2016-2945*, 2016.

[13] Brown, C. and Bridges, J., "Small Hot Jet Acoustic Rig Validation," *NASA/TM-2006-214234*, 2006.

[14] Bridges, J. and Wernet, M., "Establishing Consensus Turbulence Statistics for Hot Subsonic Jets," *AIAA Paper 2010-3751*, 2010.

[15] Ffowcs Williams, J. E. and Hawkings, D. L., "Sound Generated by Turbulence and Surfaces in Arbitrary Motion," *Philosophical Transactions of the Royal Society of London, Series A*, Vol. A264, No. 1151, 1969, pp. 321–342.

[16] Lockard, D. P., "An Efficient, Two-Dimensional Implementation of the Ffowcs Williams and Hawkings Equation," *Journal of Sound and Vibration*, Vol. 229, No. 4, 2000, pp. 897–911.

[17] Mancinelli, M., Pagliaroli, T., Marco, A. D., and Camussi, R., "Wavelet decomposition of hydrodynamic and acoustic pressures in the near field of the jet," *Journal of Fluid Mechanics*, Vol. 813, No. 25, 2017, pp. 716–749.

[18] Chen, H., Kandasamy, S., Orszag, S. A., Succi, S., and Yakhot, V., "Extended Boltzmann Kinetic Equation for Turbulent Flows," *Science*, Vol. 301, No. 5633, 2003, pp. 633–636.

[19] Chen, H., Orszag, S., Staroselsky, I., and Succi, S., "Expanded Analogy Between Boltzmann Kinetic Theory of Fluid and Turbulence," *Journal of Fluid Mechanics*, Vol. 519, Nov. 2004, pp. 301–314.

[20] Yakhot, V. and Orszag, S. A., "Renormalization Group Analysis of Turbulence. I. Basic Theory," *Journal of Scientific Computing*, Vol. 1, No. 1, 1986, pp. 3–51.

[21] Yakhot, V., Orszag, S. A., Thangam, S., Gatski, T. B., and Speziale, C. G., "Development of Turbulence Models for Shear Flows by a Double Expansion Technique," *Physics of Fluids A*, Vol. 4, No. 7, 1992, pp. 1510–1520.

[22] Casalino, D., Ribeiro, A. F. P., Fares, E., Nölting, S., Mann, A., Pérot, F., Li, Y., Lew, P.-T., Sun, C., Gopalakrishnan, P., Zhang, R., Chen, H., and Habibi, K., "Towards Lattice-Boltzmann Prediction of Turbofan Engine Noise," *AIAA Paper 2014-3101*, 2014.

[23] Zhang, R., Fan, H., and Chen, H., "A Lattice Boltzmann Approach for Solving Scalar Transport Equations," *Philosophical Transactions of the Royal Society A: Mathematical, Physical and Engineering Sciences*, Vol. 369, 2011, pp. 2264–2273.

[24] Chen, H. and Zhang, R., "Computer Simulation of Physical Processes," 2011, US Patent App. 13/151,221.

[25] Chen, H., Zhang, R., and Gopalakrishnan, P., "Lattice Boltzmann Collision Operators Enforcing Isotropy and Galilean Invariance," 2017, US Patent App. 9/576,087.

[26] Casalino, D., "An Advanced Time Approach for Acoustic Analogy Predictions," *Journal of Sound and Vibration*, Vol. 261, No. 4, 2003, pp. 583–612.

[27] Farassat, F. and Succi, G. P., "The Prediction of Helicopter Discrete Frequency Noise," *Vertica*, Vol. 7, No. 4, 1983, pp. 309–320.

[28] Mollo-Christensen, E., "Jet Noise and Shear Flow Instability Seen from an Experimenters Viewpoint," *Journal of Applied Mechanics*, Vol. 34, 1967, pp. 1–7.

[29] Jordan, P. and Colonius, T., "Wave Packets and Turbulent Jet Noise," *Annual Review of Fluid Mechanics*, Vol. 45, 2013, pp. 173–195.

[30] Ffowcs Williams, J. E. and Maidanik, G., "The Mach Wave Field Radiated by Supersonic Turbulent Shear Flows," *Journal of Fluid Mechanics*, Vol. 21, 1965, pp. 641–657.

[31] Ribner, H. S., *Aerodynamic Sound from Fluid Dilatations: A Theory of the Sound from Jets and Other Flows*, Institute of Aerophysics, University of Toronto, 1962.

[32] Ffowcs Williams, J. E., "Hydrodynamic Noise," *Annual Review of Fluid Mechanics*, Vol. 1, 1969, pp. 197–222.

[33] Witze, P. O., "Centerline Velocity Decay of Compressible Free Jets," *AIAA Journal*, Vol. 12, No. 4, 1974, pp. 417–418.

[34] Mendez, S., Shoeybi, M., Lele, S. K., and Moin, P., "On the Use of the Ffowcs Williams-Hawkings Equation to Predict Far-Field Jet Noise from Large-Eddy Simulations," *International Journal of Aeroacoustics*, Vol. 12, No. 1–2, 2013, pp. 1–20.

[35] Housman, J., Stich, G., Kiris, C., and Bridges, J., "Jet Noise Prediction using Hybrid RANS/LES with Structured Overset Grids," *23rd AIAA/CEAS Aeroacoustic Conference*, Vol. 3213, 2017, pp. 1–21.

[36] Pauz, V., Niemoller, A., Meinke, M., and Schroder, W., "Numerical analysis of chevron nozzle noise," *23rd AIAA/CEAS Aeroacoustic Conference*, Vol. 3853, 2017, pp. 1–16.

[37] Hoarau, Y., Peng, S.-H., Schwamborn, D., and Revell, A., *Progress in Hybrid RANS-LES Modelling*, Springer, 2016.

[38] Angelino, M., Xia, H., Moratilla-Vega, M., and Page, G., "Far-field Noise Prediction of Round and Serrated Jets with Increasingly Refined Grids," *22nd AIAA/CEAS Aeroacoustic Conference*, Vol. 3047, 2016, pp. 1–12.

[39] Depuru-Mohan, N. and Dowling, A., "Jet-Noise-Prediction Model for Chevrons and Microjets," *AIAA Journal*, 2016, pp. 3928–3940.

[40]Xia, H., "Turbulent jet characteristics for axisymmetric and serrated nozzles," *Computer and Fluids*, Vol. 110, 2015, pp. 189–197.

[41]Aikens, K., Dhamankar, N., Martha, C., Situ, Y., Blaisdell, G., Lyrintzis, A., and Li, Z., "Equilibrium Wall Model for Large Eddy Simulations of Jets for Aeroacoustics," *52nd Aerospace Science Meeting*, Vol. 0180, 2014, pp. 1–22.

[42]Benderskiy, L. and Lyubimov, D., "Investigation of Flow Parameters and Noise of Subsonic and Supersonic Jets using RANS/ILES High Resolution Method," *29th Congress of the International Council of the Aeronautical Science, St.Petersburg, Russia*, 2014, pp. 1–9.

[43]Grizzi, S. and Camussi, R., "Wavelet Analysis of Near-Field Pressure Fluctuations Generated by a Subsonic Jet," *Journal of Fluid Mechanics*, Vol. 698, 2012, pp. 93–124.